Interfacial damage based life model for EB-PVD thermal barrier coating

C. Courcier, Vincent Maurel, L. Rémy, S. Quilici, I. Rouzou, A. Phelippeau

Interfacial damage based life model for EB-PVD thermal barrier coating

C. Courcier [1,2], V. Maurel [1], L. Rémy [1], S. Quilici[1], I. Rouzou[1], A. Phelippeau[2]

[1] *Centre des Matériaux, Mines ParisTech, UMR CNRS 7633*
BP 87, F-91003 Evry Cedex, France
[2] *SNECMA/SAFRAN Group YQM*
rond point René Ravaud, F-77550 Moissy-Cramayel, France

Abstract

Thermal barrier coating life modelling is a major challenge for industrial applications. This study aims to highlight critical damage mechanisms involved in TBC failure for both isothermal and cyclic oxidation conditions. Experimental database is analysed in relation to elastic buckling of the ceramic top coat obtained by mechanical compressive tests. Ageing is modelled thanks to an original damage approach dealing with the evolution of interfacial properties and loading history. This methodology is successfully applied as a post-processor to a 3D blade simulation for typical thermo-mechanical fatigue in-service loading.

Keywords: EB-PVD Thermal barrier coatings, interfacial damage model, Thermomechanical Fatigue, Analytical modeling

1. Introduction

Turbine efficiency improvement requires gas inlet temperature increase. Thermal barrier coating (TBC) systems have been used for over twenty years for hot blades in advanced gas turbines, in aero-engines as well as power-plants, to protect the substrate from both high temperature transient and

Email address: vincent.maurel@mat.ensmp.fr (C. Courcier [1,2], V. Maurel [1], L. Rémy [1], S. Quilici[1], I. Rouzou[1], A. Phelippeau[2])

environmental effects. For air-cooled blades, the cooling is improved by a ceramic top coat (TC) layer, stuck to the substrate by a bond coat (BC) layer. The latter is used as an Aluminium reservoir to create an adherent and stable α-alumina scale between ceramic top coat and metallic bond coat layers. This thermal grown oxide (TGO) reduces diffusion rate from the substrate and thus protects it from detrimental oxidation. Nevertheless, TBC systems are subjected in service to severe thermal-mechanical fatigue loading and they may break by spallation of large areas of the ceramic layer after long term operation. The integrity of the TBC is therefore a major concern in the design of advanced turbine blades.

Macroscopic spallation is triggered by maximum in-plane compressive stress and the decrease in ceramic/metal interface toughness due to ageing effects [1]. Large scale buckling (LSB) [2, 3] is mostly activated in the low temperature stage of the loading path [4]. On the other hand interfacial damage is known to be a combination of microstructure evolution linked to the growth of the alumina scale, which is thermally activated, and roughness evolution, the so-called rumpling effect, induced by thermal cycling [3, 5, 6]. Therefore damage mechanism linked to oxide growth is a direct function of the time spent at high temperature whereas the damage linked to roughness evolution will evolve with cyclic frequency [1, 7].

Based on experimental studies of cyclic oxidation, the currently admitted scenario of spallation occurs in four different stages [1, 6]: i) damage of the ceramic/metal interface, ii) delamination initiated on existing defaults or damaged area, iii) buckling of the top coat and iv) macroscopic spallation, Fig. 1. This scenario needs to be confirmed experimentally. However, it is very difficult to assess the relative importance of buckling, induced delamination and dynamic spallation as the observations are mostly post-mortem. Indeed, the damage and final failure of the system involves multiple time scales: for the evolution of damage and delamination of the system interfaces, the time period ranges from a few minutes to several hundreds hours, whereas final spallation can be unstable in fractions of seconds. TBC system damage is initiated at the ceramic/metal interface, considered to be the micro-scale analysis that involves roughness values (Ra) of about a few micrometres. Damage propagation will drive the system to delaminate over several tenths of microns up to a scale of one millimetre, leading to final spallation events that range from one millimetre to a few centimetres, thus making the problem also multi-scaled in space.

The observations of interfacial roughness by many authors have stimu-

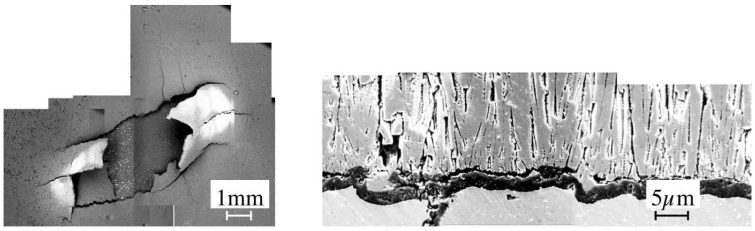

(a) (b)

Figure 1: SEM micrograph of spalled TBC by compressive mechanical test performed at 750°C a) macroscopic spallation on specimen surface b) cross-section showing delamination at top coat/oxide interface

lated a lot of analytical and finite element analysis of interfacial elementary pattern assuming a perfect periodicity of the interfaces [8, 9**?** , 10]. Moreover, many authors address TBC systems life assessment using a direct local approach based on the evaluation of a local state, leading to a binary evaluation of the TBC system state : safe or spalled. Those models could be based on a critical oxide thickness [11] or oxide net mass gain [12, 13, 14], a damage parameter function of the maximum local stress [**?**] as well as the evaluation of a maximum stress intensity factor (SIF) in a linear elastic fracture mechanics (LEFM) scheme [2, 15, 16, 17, 18].

But experiments show that even if cracks are present locally, the top coat layer could stay adherent. This point makes the above approaches less easy to defend and quite difficult to validate. Moreover, cracks in the TGO layer could be healed at high temperature: specific thermo-mechanical fatigue (TMF) loading condition could lead, without macroscopic breakdown, to a greater oxide thickness than critical thickness evaluated for isothermal loading [19, 20]. However in service, components are subjected to both high and low temperature stages, with frequency variations, and in which maxima reached for thermal and mechanical loading could be non-synchronous. Thermo-mechanical fatigue (TMF) tests are therefore known to be the most relevant manner to mimic in-service loading conditions, combining thermal and mechanical loading with phasing effects [19, 21, 22, 23**?** , 5].

In the scope of local models, many authors have tried to estimate local mechanical states for each layer, taking into account as far as possible microstructure morphology and local behaviour [9, 24, 25]. Despite many efforts

due to the extreme thinness and complexity of the material, both microstructural evolution and relevant behaviour determination are still challenging tasks [26, 27].

To assess microstructure evolution, many authors propose using cyclic oxidation database and correlated models based on remaining chemical potential in the BC layer in order to estimate TBC lifetime [28]. This class of model is mostly restricted to a given cycle frequency and could hardly describe mechanical interaction [13].

Cycling effects also occur during the highest temperature regime. But the typical maximum in plane compressive stress and maximum out-of-plane stress is obtained for the lowest temperature due to maximum thermal expansion mismatch between the different layers constituting the TBC system. Moreover, interfacial damage is known to be mostly thermally activated, whereas macroscopic spallation is an a priori brittle mechanism mostly reached in the low temperature regime.

An alternative method to these local models is the evaluation of a continuous interfacial properties evolution and a final test procedure of the critical event encountered during loading. The pioneer works of Miller et al. and Cruse et al. for air plasma sprayed TBC help to build fundamentals of the methodology herein [29, 30]. The author's proposal was to assess plasma sprayed TBC lifetime thanks to a competition between oxidation and mechanical driven failure [31]. For APS-TBC, phenomenological relevant models could also be based on the distinction between incubation time for crack propagation and final failure [18].

For engineering purposes, it seems necessary to have a simple and robust approach in order to assess the life of EB-PVD TBC systems. As the EB-PVD TBC final spalling off is unstable and is mostly promoted by the low temperature part of the loading, our approach focuses on the evolution of damage that occurs due to high temperature exposure under oxidising conditions and during thermal transients. This classification relies on detailed observations made by other authors and in our group on aluminide coatings and TBC systems [5, 32, 33, 4].

Cyclic oxidation data are used as a basis to obtaining tests giving rise to TBC spallation. Oxidation was also found to depend upon temperature cycles: isothermal, cyclic or with a superimposed mechanical strain [34, 19]. On the other hand simple compression tests were used to measure the evolution of resistance to TBC spallation as a function of the number of oxidation cycles prior to failure [34, 35]. This framework provides access to a critical

compressive strain to failure, used as an average measurement of TBC resistance to delamination and spalling. Such tests were also used to assess the evolution of this resistance to spalling for different isothermal exposure times at high temperature.

The paper is organised as follows: firstly test results from compression straining after different amounts of prior oxidation under static conditions and secondly the results of cyclic oxidation tests, interrupted and conducted to spalling of the EB-PVD TBC, are summarised. Then a two-step post-processing model is used to describe the damage kinetics: firstly, a simple multi-layer model based on the constitutive behaviour of individual layers is proposed to estimate the mean mechanical state in each layer, secondly a damage model is identified using the mechanical quantities so computed and the database. The damage kinetics is mainly estimated from compression tests after oxidation of specimens. The lifetime of TBC spallation is then evaluated for specimens and finally compared with information available on real blades tested using accelerated engine test conditions.

2. Experimental procedure

For in service conditions, components are subjected to Thermo-Mechanical Fatigue loading that should be accounted for in the database design. A typical loading path for aero-turbine blade substrate is drawn in Fig. 2a) in the stress/temperature space completed for temperature only as a temperature/time function, Fig. 2b). The substrate loading cycles - typical diamond like TMF cycles - are subjected to variations of mean stress as a function of the location in the blade. The vertical arrows represent mean stress evolution from positive to negative values as well as extreme evolution leading to strong differences in the BC microstructure evolution [**?**]. Loading in the TC layer is estimated and plotted Fig. 2. Assumptions used for this calculationare detailed later on. The TC layer undergoes high level of compression for the lowest temperature whereas thermal fatigue will affect each layer of the TBC system. Hence, the present methodology aims to discriminate ageing effects, arising at both high and low temperature stages, from final catastrophic failure at low temperature. The former is known to be linked to microstructure evolution inducing the decrease of metal/ceramic interface toughness. The latter is driven by mechanical effect at the macroscopic scale that becomes critical due to increasing thermal mismatch with system cooling. The procedure is thus divided into two stages. Firstly an ageing stage is applied to

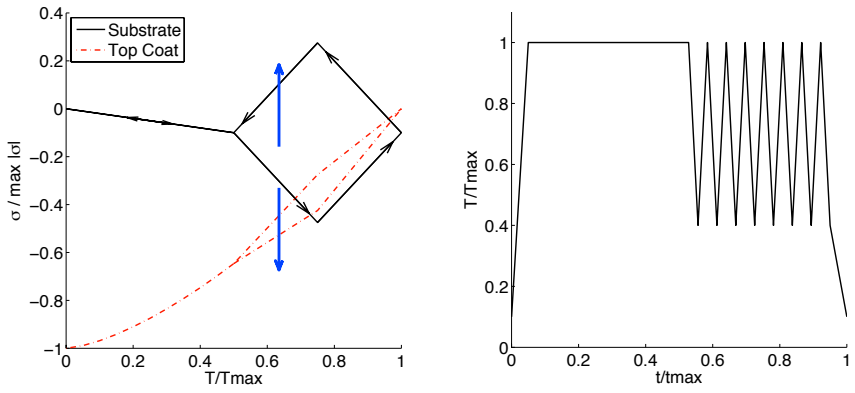

(a) (b)

Figure 2: Typical thermal-mechanical fatigue loadingpath for turbine blade in service. a) stress loading versus temperature. Vertical arrows indicate the loading variation depending on the location on surface blade. b) thermal loading versus time

the specimen for isothermal as well as cyclic thermal loading. Secondly a mechanical compressive test is applied up to top coat spallation. The critical strain reached at spallation is measured and allows estimation of ageing influence on the damage of the TBC system. This approach enables the use of interrupted tests and therefore a precise and relevant assessment of interfacial damage evolution. Interrupted tests are also important for ascertaining the physics of TBC system ageing. Interfacial damage main features will be addressed for both isothermal and cyclic thermal loading.

2.1. Material and specimens

The substrate material is a nickel-based single crystal superalloy AM1 processed by Snecma - Safran Group for aero-engine blades, the composition of which is detailed in table 1. An oxidation protection layer is deposited over the substrate. This bond coat is a platinum enriched aluminide overlayer (Ni,Pt)Al. This low energy coating is deposited by pack-cementation, and presents a duplex layer aspect as previously observed [35]. The outer layer is mostly composed of beta-NiAl phase, whereas the inner layer contains a large number of precipitates. The beta-NiAl phase composition is detailed in table 2. A short pre-oxidation forms a thin TGO layer before final EB-PVD coating with a Y_2O_3 partially stabilised zirconia coating. This typical

columnar structure measures approximately 100μm in thickness. Coatings are processed by the Ceramic Coating Centre (CCC) / Snecma - Safran Group. Large scale TBC spallation imposes the use of homogeneous stress

Table 1: Chemical composition (in Wt%) of single crystal nickel-base superalloy AM1 at room temperature [36]

	Ni	Co	Cr	Mo	W	Ta	Al	Ti	C	Fe	S
Min	bal.	6	7	1.8	5	7.5	5.1	1			
Max	bal.	7	8	2.2	6	8.5	5.5	1.4	0.01	0.2	0.2ppm

Table 2: Chemical composition (in At%) of Ni(Pt,Al) Bond Coat layer in the as-received condition [37]

Al	Pt	Cr	Co	Ni	Ti	Ta	Mo	W
35.2	7.3	1.0	4.6	42.0	0	1.0	0.	0.

cylindrical test specimens, the geometry of which is detailed elsewhere [38, 39]. All specimens have undergone isothermal or cyclic high temperature pre-oxidation to study the coating's adherence. TBC coated specimens were isothermally oxidised in tube furnaces at 1100°C ($\pm$ 3°C) and air-cooled. The isothermal dwell times were chosen in order to produce a thick and continuous alumina scale, while avoiding any spallation upon cooling. Furnaces and air cooling were also used for thermal cycling.

Mechanical tests are all strain controlled. Lamp furnaces were used to control specimen temperature during compressive tests. SEM observation of the rupture interface yields information on the evolution of the interfacial toughness of the system.

2.2. Interrupted tests for isothermal ageing condition

The aim of this section is to address the evolution of the ceramic/metal interface damage with time spent at high temperature for isothermal loading condition. The chosen methodology is based on the assumption that the ageing phenomenon could be distinguished from the final failure of the system experienced at the low temperature stage.

Thus, first step of the procedure is a high temperature stage in order to promote interfacial damage during isothermal loading. For specimens that are not spalled on the first cooling after the ageing stage, a strain controlled compressive mechanical test is performed. TBC delamination marks the end of the test and enables to identify a critical strain. Therefore the critical strain reached at spallation is evaluated as a decreasing function of the time spent at a high temperature, Fig. 3 [40].

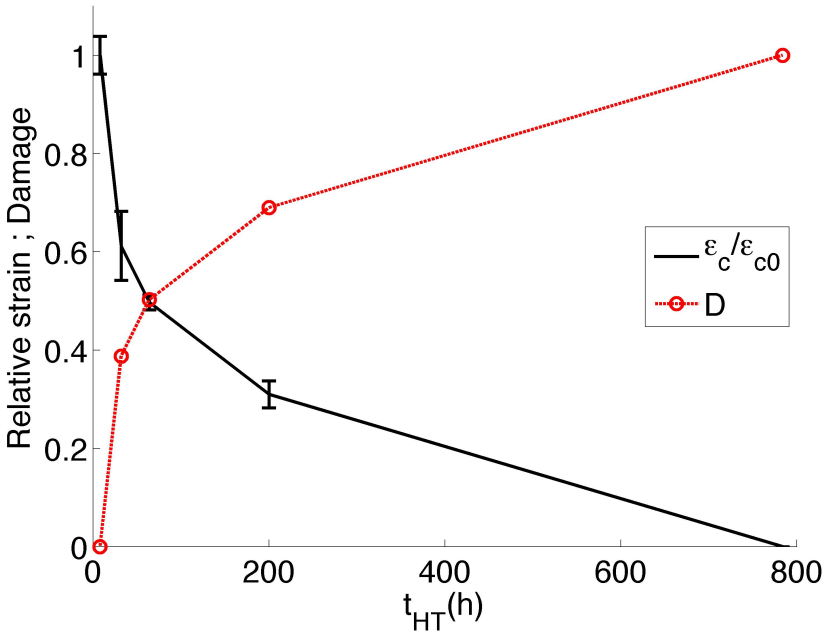

Figure 3: Normalisedcritical strain obtained for TBC spallation under compressive loading at room temperature as function of isothermal ageing dwell time. Error bars correspond to standard deviation of critical strain normalised by initial critical strain ε_{c0}. The extrapolated damage function is evaluated according to eq. 8

At a lower scale, SEM analysis provides information about the damage mechanism activated by the isothermal loading. For the as-processed specimen or short time exposure at high temperature, delamination is known to be localised at the top coat/oxide interface as a consequence of crack initiation on voids due to local roughness that could be seen as an initial damage state [41]. By increasing the holding time at high temperature, the location

of failure moves progressively from the top coat/oxide to the oxide/bond coat interface, Fig. 4. This phenomenon is assumed to be a direct consequence

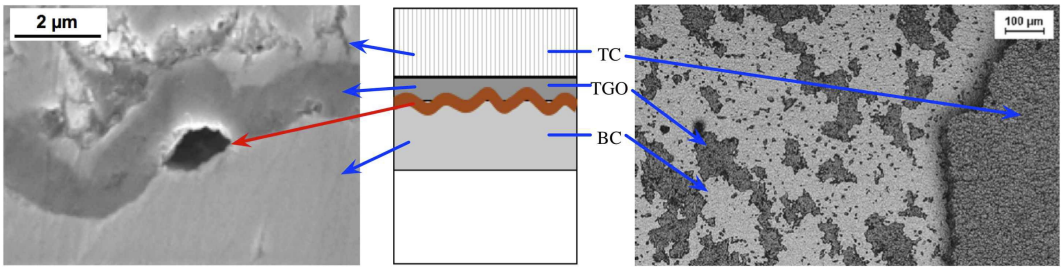

Figure 4: SEM micrograph of spalled TBC by compressive mechanical test performed at 20°C a) SEM cross-section of typical void at the BC/TGO interface. b) sketch of the multi-layered TBC system cross-section with highlighted damaged interface in red. c) SEM top-view of a spalled area mixing TGO (dark) and BC (bright). The top coat is only visible on the right.

of Al and vacancies diffusion [6]. Indeed, the high temperature stage promotes damage of oxide/bond coat interface by void nucleation, growth and coalescence known to occur during isothermal loading [35]. It could be supposed that the top coat/oxide interface toughness remains almost constant whereas the damage level of oxide/bond coat interface strongly increases with isothermal loading. This point could explain the displacement of the weak interface.

In order to test the influence of bond coat viscosity in the spallation process, tests have been made for the same ageing time at high temperature but for different temperatures with the mechanical test. The first remarkable feature of a compressive test with increasing temperatures, is the drastic increase in the level of critical strain up to 950°C where no spallation was observed [4].

The damage pattern is also modified with increasing temperatures. For a low temperature, delamination is initiated at oxide/bond coat interface - which is coherent with the above results: at 20°C, surface SEM observation of the spalled area makes the bond coat surface, which appears as the lighter parts of the area, more visible Fig. 4. With increasing temperatures, the weak interface moves from oxide/bond coat to top coat/oxide interface: at 750°C, the dark rupture interface denotes damage propagation closer to the top

coat/oxide interface, Fig. 5. Bond coat creep properties should beinvolved

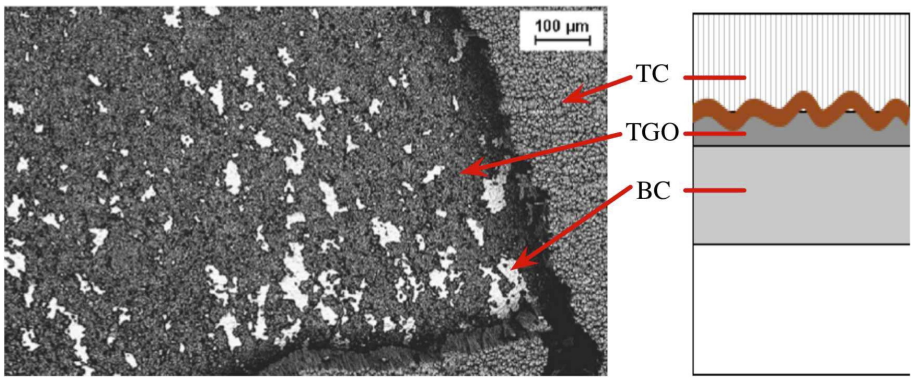

Figure 5: SEM micrograph of spalled TBC by compressive mechanical test performed at 750°C a) SEM top-view of a spalled area mixing TGO (dark) and BC (bright) b) sketch of the multi-layered TBC system cross-section with highlighted damaged interface in red.

in this phenomenon. Indeed, at low temperatures both top coat/oxide and oxide/bond coat interfaces are brittle. Because the diffusion process is activated at a high temperature the dwell-time will therefore only damage the oxide/bond coat interface. With a higher temperature up to 950°C, where the temperature is considered low enough to neglect bond coat oxidation, top coat/oxide interface is still brittle whereas the oxide/bond coat interface experiences lower stresses since they are relaxed by bond-coat creep. Large scale buckling is therefore sensitive to the contrast between bond coat and oxide viscosity and top coat elasticity, carefully detailed elsewhere [4].

In conclusion, the critical strain to be accounted for spallation is a decreasing function of time spent at high temperature. The damage is mostly located at the oxide/bond coat interface for isothermal loading. Spallation could only occur, with reliable compressive strain value, at a low temperature. This last point justifies the distinction made between local damage and final macroscopic failure.

2.3. Cyclic oxidation

In service loading exhibits fatigue stages with both mechanical and thermal cycling effects. The essential feature that differs in cyclic oxidation from

isothermal loading is the exertion of the so-called rumpling effect [42, 43]. The rumpling phenomenon consists of the increase of oxide and bond coat roughness with the number of thermal cycles. But the ceramic top coat is not compliant enough to follow this roughness evolution. Therefore, voids and microcracks will develop at the ceramic/oxide interface [44].

Standard 1-hr thermal fatigue cycles are used to address macroscopic failure of TBC systems with cycle numbers [45]. Unfortunately, typical aero-engine service loadings involve shorter dwell time at high temperature than standard cycles. This assumption is ascertained by experimental damage modes obtained with relative high frequency cyclic testing closer to in-service damage modes than with standard 1-hr cycles [**?**].

Frequency effect is of major concern [7] as the dwell-time at high temperatures and the number of cycles will greatly affect the damage rate of the system, Fig. 6 [46]. The frequency effect is tested at 1100Â°C for a 15-mn high temperature hold time cycle compared to the standard 1hr-cycle. The average number of cycles to failure increases, $N_f(15mn) \simeq 2N_f(1hr)$ whereas the cumulated time spent at high temperature decreases, $t_{HT}(15mn) \simeq 1/2t_{HT}(1hr)$.

Temperature effect is addressed varying the maximum temperature reached in cyclic testing from 1100 to 1150°C. The decrease of the number of cycles to failure is clearly addressed with increased temperature. This effect could be linked to both a higher TGO thickness and an overall stronger activation of the diffusion process.

Such tests are completed with interrupted tests done over 1hr-cycles at 1100Â°C. The methodology is the same as the one done for isothermal loading: cyclic loading is first applied on the specimen as an ageing stage followed by a compressive mechanical test performed at room temperature.

Even if the rumpling effect is known to be the result of microstructure evolution driven by thermal cycling, the physics of rumpling is still a controversial issue [47]. Nevertheless, rumpling could be assumed to be a combination of diffusion, creep and coefficiency of thermal expansion mismatch between oxide, bond coat layers and substrate [7]. The phase transformation in the BC also seems to greatly influence rumpling phenomenon[48]. Finally, mechanical ratchetting at the low temperature stage contributes as a major factor to roughness increase as soon as the mechanism is initiated. For processes where the roughness of the TBC system is above a few microns the rumpling will be initiated on small voids or typical oxide ridges, that is to say defaults related to the EBPVD process and surface finishing [49]. For the

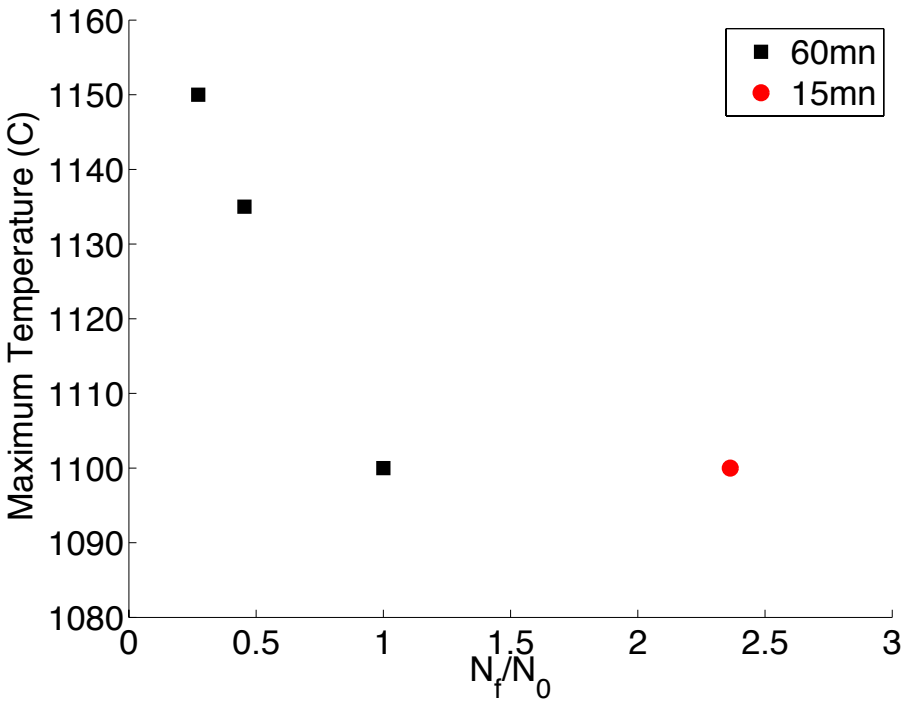

Figure 6: Normalisedmean values of cycles to failure as a function of maximumtemperature and dwell timefor cyclic oxidation experiment.

system studied, this point is confirmed and could be related to a fairlyhigh level of initial roughness, Fig. 7. Moreover, for coated systems without ceramic top coat the increase of roughness with cyclic oxidation is much higher than for systems with ceramic top coat, due to free surface effect. If voids exist in the presence of ceramic top coat, the out-of-plane displacement could be pronounced. The rumpling phenomenon affects the oxide and bond coat roughness without causing much impact on ceramic flatness. Ceramic adherence seems to be only insured at the peak of oxide local roughness allowing delamination induced bydownward motion of the remaining oxide surface. Therefore, in cyclic oxidation the weak interface is the top coat/oxide, which is prone to increasing delamination and an increased rumpling effect, Fig.7.

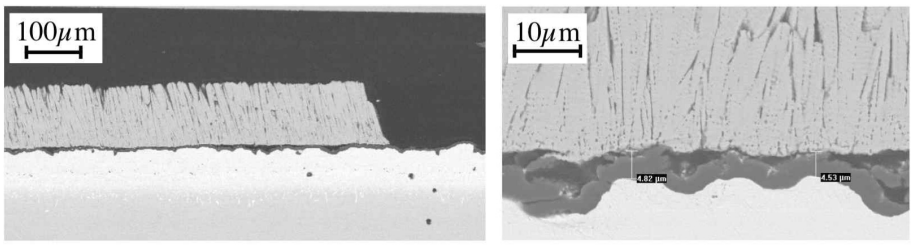

Figure 7: SEM micrograph of spalled TBC for thermal cycling test performed at 1135°C a) Cross section showing the top coat spallation location b) Detail of the oxide (dark) roughness and progressive separation of the top coat by top coat/oxide interfacial damage [46]

3. Damage based macroscopic life model

TBC system life assessment needs to deal with both progressive interfacial damage increase and fast final macroscopic spallation of the ceramic layer. The above database is designed to estimate the mechanical critical strain before the final breakdown of the system for isothermal as well as cyclic thermal loading. Interfacial damage evolution is thus estimated through interrupted tests. The final failure of the system is described through an elastic buckling analysis of the top coat layer. A macroscopic damage parameter is therefore used to indicate the decrease of critical strain with ageing observed experimentally.

This methodology allows to distinguish the ageing stage, involving a micro scale related to oxide interfaces, from macroscopic buckling-spallation at the macroscopic scale. A post-processing approach allows versatility of the model for 3D finite element analysis (FEA) of industrial components. In such a situation, all mechanical quantities used as model input are related to a single node of the mesh surface. Therefore all output quantities and especially spalled areas are connected to each node without any description of eventual damage propagation from a spalled area to its neighbourhood.

3.1. Mechanical state in TBC layers

The mechanical state of each layer constituting the TBC system is estimated according to a flat multilayer simulation, where the main assumptions are: i) because of the high level of substrate stiffness compared to other

layers, the strain is prescribed by the substrate to all the other layers including bond coat, oxide and ceramic top coat; ii) no explicit description of the system geometry is embedded in the model. The local roughness and especially the increase of roughness with rumpling will be implicitly described ina damage analysis of the interfaces to be discussed later on. Therefore, the following equation 1 is sufficient to estimate the average mechanical state of each layer i

$$\underset{\sim}{\boldsymbol{\varepsilon}}_i^{tot} = \underset{\sim}{\boldsymbol{\varepsilon}}_i^{th} + \underset{\sim}{\boldsymbol{\varepsilon}}_i^{m} = \underset{\sim}{\boldsymbol{\varepsilon}}_{sub}^{tot} \tag{1}$$

where ε_i^{tot}, ε_i^{th} and ε_i^m are respectively total, thermal and mechanical strain of the considered layer i. ε_{sub}^{tot} refers to the substrate strain. The subscribpt $\underset{\sim}{}$ refers to mechanical tensor. When the system undergoes the EB-PVD deposition process, it is assumed that there is neither mechanical strain nor stress in the system. Thus a correction is applied for thermal strain computation to describe cooling fromprocess temperature

$$\varepsilon_i^{th}(T) = \alpha_i(T)(T - T_0) + [\alpha_{sub}(T_{pro}) - \alpha_i(T_{pro})](T_{pro} - T_0) \tag{2}$$

where the coefficient of thermal expansion, $\alpha_i(T)$, is estimated for each layer i as a function of temperature T, with a process temperature $T_{pro} \simeq 1100°\mathrm{C}$ and a reference temperature T_0. The thermal strain tensor is assumed to be isotropic for each layer $\underset{\sim}{\boldsymbol{\varepsilon}}_i^{th} = \varepsilon_i^{th}\underset{\sim}{\mathbf{1}}$.

The bond coat behaviour is assumed to be isotropic and is described as elasto-visco plasticity with a non linear kinematic hardening model, see table 3, with no description of phase transformation and induced behaviour evolution [50, 51]. The oxide is modelled through thermo-viscoelasticity and growth strain is not taken into account [52]. The ceramic top coat is assumed to be elastic transversally isotropic [34, 1, 35, 51, 9]. The top coat sintering effect is assumed to be negligible for our system when used in aero-engines due to the relatively short life and high temperature dwell time in comparison to land-based gas-turbines where this phenomenon could affect top coat behaviour. Elastic temperature dependent parameters are detailed intable 4.

3.2. Failure Analysis

This point is related to the life of the system estimated at a macroscopic scale. The top coat layer is modelled by an equivalent delaminated area considered as a circular blister prone to buckling. The critical stress, σ_{crit}, is predicted by the classical Euler buckling theory for elastic analysis. It is

Table 3: Governing equations of the Lemaitre and Chaboche model [53] used for Ni(Pt,Al) Bond Coat layer [51]

Flow rule	$\dot{\varepsilon}_p = \left(\frac{\|\|\sigma - \sum_i X_i\|\| - R_0}{K}\right)^n$
Yield stress	R_0
Kinematic hardening	$X_1 = \frac{C_1}{D_1}(1 - e^{-D_1\varepsilon_p})$
	$X_2 = C_2\varepsilon_p$

Table 4: In plane Young Modulus (E), Poisson ratio (ν) and Coefficient of Thermal Expansion (CTE) when used for the different layers at 20 and 1100°C [50, 54]

Material	E (GPa)		ν	CTE (10^{-6}/°C)	
T°C	20	1100		20	1100
Top coat ($Zr0_2$)	50	20	0.2	10	10
Bond coat (Ni(Pt,Al))	188	145	0.3	11	15
Substrate (AM1)				8	16

assumed that there is a homogeneous distribution of the loading for a circular blister with clamped boundary conditions where the stress state is uniform, equi-biaxial compression σ [55, 56, 57], eq. 3

$$\sigma_{crit} = 1.2235 \frac{E_1}{1 - \nu_1^2} \left(\frac{h}{R}\right)^2 \tag{3}$$

where E_1 and ν_1 are respectively in-plane Young modulus and Poisson ratio of the ceramic top coat layer. As delamination is localised at the ceramic/metal interface, the thickness of the circular blister is assimilated to the top coat thickness $h = h_{TC}$. The critical stress to be accounted for should be affected by the decrease of interfacial adherence with ageing. Thus a macroscopic damage parameter D is introduced in eq. 3 enabling a decrease of critical stress

$$\sigma_{crit} = 1.2235 \frac{E_1}{1 - \nu_1^2} \left(\frac{h}{R_0}\right)^2 (1 - D) \tag{4}$$

where R_0 is the initial radius of the equivalent delaminated area prone to buckling. This equation leads to zero critical stress for complete interfacial

damage, i.e. $D = 1$. Indeed, the radius of the circular blister to be considered is virtually increased with D value, eq. 5

$$R = \frac{R_0}{\sqrt{1-D}} \tag{5}$$

and the corresponding damaged surface moves from S_0 to S following eq. 6

$$S = \frac{S_0}{1-D} \tag{6}$$

that differs from the classical damage theory [58, 53] because the delaminated surface S would tend to infinity with a damage parameter reaching 1. This breakdown value corresponds to spontaneous buckling of the ceramic layer area related to the averaged surrounding finite element area of the node where eq. 3 is evaluated. As has been said, all tests are performed under strain control, therefore criticality of the system is analysed in this situation turning stress, eq. 3, into strain by classic elastic analysis that is coherent with assumptions made for buckling. On the whole, the stress state is assumed to be uniform equi-biaxial compression leading to critical strain ε_{crit}, eq. 7

$$\varepsilon_{crit} = \frac{1.2235}{1+\nu_1}\left(\frac{h}{R_0}\right)^2(1-D) \tag{7}$$

where all parameters are the same as above. This equation addresses the scale transition between final macroscopic failure and interfacial delamination triggered by ageing effects and modelled by the damage term D. The system failure is related to the following condition: the system fails if the maximum absolute value of the compressive strain exceeds the critical strain ε_{crit}.

3.3. Interfacial damage

Experiments reveal the global metal/ceramic interfacial damage increase with ageing. This effect is modelled usinga global damage parameter D, introduced in eq. 4. This damage parameter enables the inverse identification of system loss of adherence due to ageing effect according to

$$D = 1 - \frac{1+\nu_1}{1.2235}\left(\frac{R_0}{h}\right)^2\varepsilon_{crit} \tag{8}$$

This damage evolution is plotted for isothermal conditioning Fig. 3.

Depending on loading conditions, damage evolution at the different failure interfaces should be modelled. Only bond coat/TGO and TGO/top coat

interfaces are considered with neither description of inside TGO cracking nor transition between interfaces. The chosen macroscopic scale for buckling analysis coupled with damage prescribes the choice of a global macroscopic damage parameter. This damage is first estimated as a function of isothermal oxidationthen of cyclic oxidation.

For isothermal loading or high temperature dwell-time for TMF loading, TBC lifetime is highly correlated with TGO thickness [11, 59]. This effect is linked to segregation and a sequence of nucleation, growth and coalescence of cavities at bond coat surface. The oxide thickness should therefore be evaluated as a function of time and temperature following Wagner's theory [60]. The total thickness h_{ox} of the oxide layer at the current time is then computed from phenomenological oxide growth kinetics in terms of temperature and time t, eq. 9

$$dh_{ox} = \frac{\alpha_0}{2} \exp\Big[- \frac{Q}{RT} \Big] \frac{dt}{h_{ox}} \tag{9}$$

where α_0 is a proportionality constant, t the current time, Q an apparent activation energy and R the universal gas constant.

The fall in interfacial strength observed with isothermal oxidation tests is modelled by a power law function of the current oxide thickness, eq. 10

$$dD_{ox} = \frac{m}{h_0} \Big(\frac{h_{ox}}{h_0} \Big)^{m-1} dh_{ox} \tag{10}$$

where h_0 and m are model parameters. h_{ox} is estimated by integration of eq. 9 as a function of the number of cycles or as a function of time for isothermal conditions. Experimental sensitivity of time spent at high temperatures and temperature value are reproduced, using the thermally activated oxide growth kinetics, eq. 9.

The rumpling phenomenon observed for cyclic thermal loading especially affects the top coat/oxide interface with a drastic increase in local roughness leading to micro-crack growth. Rumpling will involve both bond coat viscosity at high temperature and plasticity in the low temperature range [**?** 61, 51, 47]. The latter is known to produce local strain ratcheting due to thermal expansion mismatch between TGO, bond coat and substrate leading to roughness increase. The coupling between cumulated plasticity of the bond coat ε_{cum} and oxide thickness h_{ox} is used to simulate the damage under cyclic oxidation, D_r as a function of the number of cycles N, eq. 11

$$dD_r = N\frac{m}{h_0}\left(\frac{\varepsilon_{cum}}{\varepsilon_0}\right)^n\left(\frac{h_{ox}}{h_0}\right)^{m-1}dh_{ox} + \left(\frac{\varepsilon^0_{cum}}{\varepsilon_0}\right)^n\left(\frac{h_{ox}}{h_0}\right)^m dN \qquad (11)$$

where n and ε_0 are the model parameters. Parameters m and h_0 are unchanged from above, eq. 10. ε^0_{cum} refers to the cumulated plasticity of the bond coat layer arising from the first thermal cooling after process.

Each damage term, D_{ox} and D_r respectively related to the isothermal oxidation and rumpling effect, is used as the implicit way to model the interfacial delamination process preceding TBC buckling. They are related to small scale damage whereas large scale buckling leads to macroscopic failure of the system. The homogenisation of such damage is addressed by the following damage equation 12

$$D = 1 - (1 - D_{ox})(1 - D_r) \qquad (12)$$

This model allows to discriminate isothermal from cyclic oxidation loading combined with mechanical loading. A sensitivity analysis of the frequency effect is carried out. This numerical test simulates thermal cycling with a prescribed compressive mechanical strain synchronous with high temperature dwell time. Temperature range is 20-1100°C for a maximum crompressive strain value $\varepsilon_{max} = 0.005$. As expected from experimental results, increasing the frequency leads to a more detrimental damage rate than at a lower frequency and isothermal test over the same period at a high temperature, Fig. 8.

4. Model identification and results

4.1. Model identification on uniaxial database

The use of elastic buckling analysis of the top coat layer is the key point of the above model and hence of the identification procedure. Compressive mechanical tests allow estimation of the compressive strain leading to failure for a given ageing state. Themulti-layer assumptions, eq. 1, isused to estimate the mechanical critical strain in the top coat layer, Fig. 3. The inverse equation, eq. 8, is then used to obtain the global damage D value related to the test conditions.

The first step is performed on the as-processed specimen for which the critical radius of the delaminated area, eq. 7, is identified assuming a zero initial damage state. For sake of simplicity the size-parameter R_0 is chosen

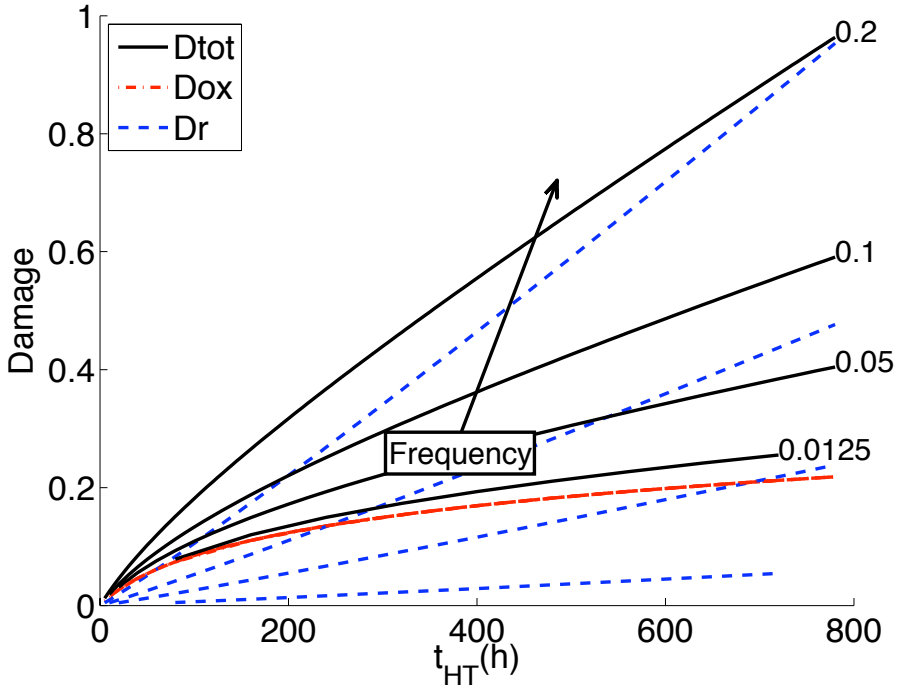

Figure 8: Frequency effect on the damage evolution for fatigue loading. Each damage term is plotted as a function of time according to equations 7 to 12., the arrow shows the effect of increasing frequency

to be consistent with the average size of the finite element mesh used in critical areas. The identification procedure is then focused on the isothermal ageing condition. Assuming that the rumpling effect could be neglected, the damage term representative of isothermal oxidation effect, D_{ox}, is equalled to the global damage parameter

$$D_{ox} = D_{ox}(t_{HT}, T) \simeq D \tag{13}$$

the parameters of eq. 10, h_0 and m are identified. A good correlation is achieved for isothermal conditions for damage, Fig. 9, and critical strain to failure, Fig. 10.

For thermal cyclic loading conditions, the knowledge of the oxidation related damage term, D_{ox}, enables the estimation of the rumpling related damage term, D_r thanks to inverse analysis, eq. 8, and total damage D, eq.12. The determination of ε_0 and n addresses the complete model identi-

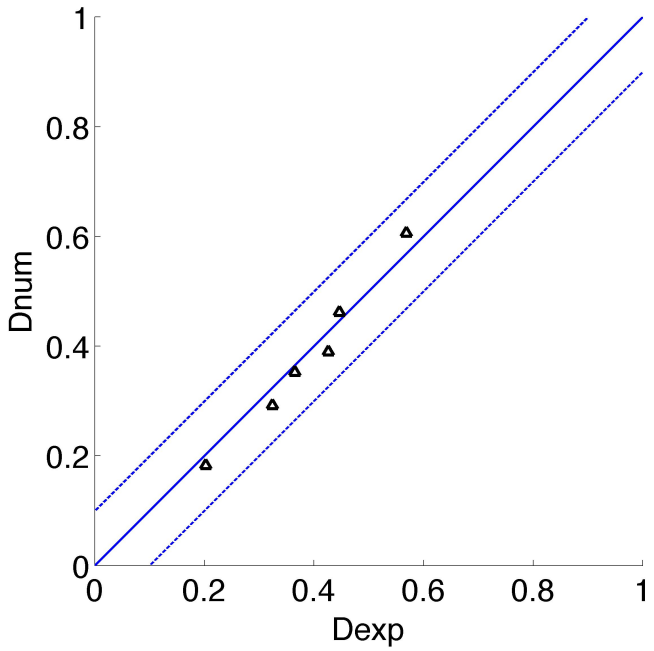

Figure 9: Model versus experiment damage valuefor isothermal oxidation(total damage analysis). Dot lines represent ±10% of error.

fication used to assess damage for the cyclic condition with good reliability, Fig. 11. This task is achieved for both interrupted tests and for tests driven to failure for cyclic loading conditions, Fig. 11. The complete model is used to assess temperature and frequency effect for cyclic oxidation, Fig. 12, that corresponds to experimental data plotted Fig. 6.

4.2. Model extension to 3D FEA

To achieve TBC life modelling for real component, e.g. next turbine blade case, the above framework should be extended to 3D FEA. The post-processing is built in the case of a typical computation whithout description of the multi-layered TBC system behaviour. The implementation involves four steps:

i) substrate surface strain, $\underset{\sim}{\varepsilon}_s$ is extracted from nodal values of the 3D FEA;

ii) the tangent plane to the surface is determined;

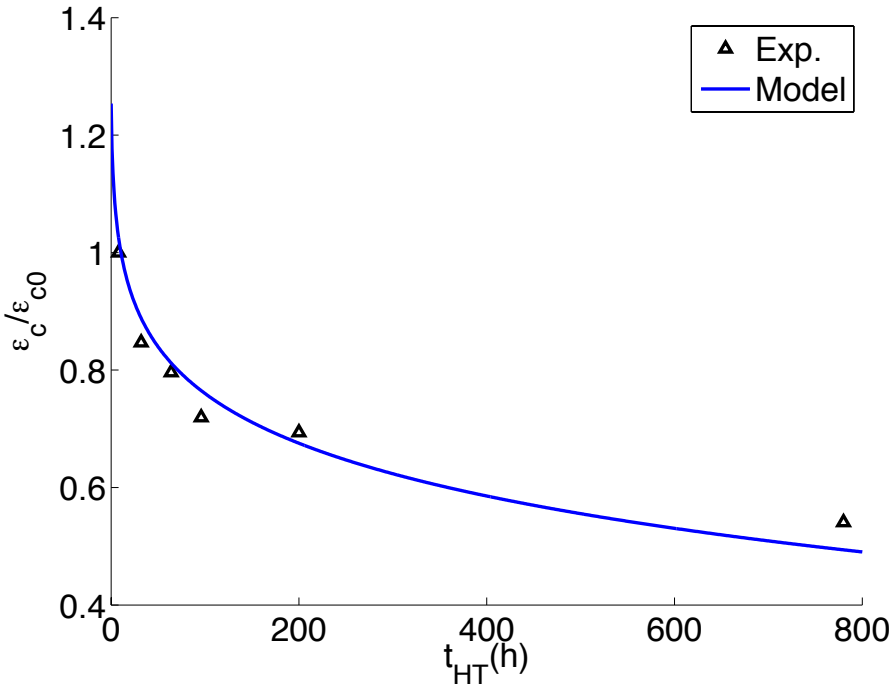

Figure 10: Critical strain vs time spent at high temperature : comparison between model and experiment for isothermal oxidation.

iii) mechanical values for each layer are computed;

iv) the damage model and failure criterion are applied on each surface node.

A major assumption of the above model is the multi-layered mechanical analysis. Indeed, each layer is assumed to be in a planar stress state. Thus the tangent plane to the substrate should be first estimated.

Local orientation of the tangent plane. The local orientation of the tangent plane in relation to the surface node of the substrate to be considered is defined with the given normal for the element plane where the node is located. Two topological cases present indetermination of the normal for the element : first, if the node is common to two different finite elements that form an angular point, Fig. 13, second if the node is associated to an edge element, Fig. 14. To prevent such indetermination, a minimisation procedure of the

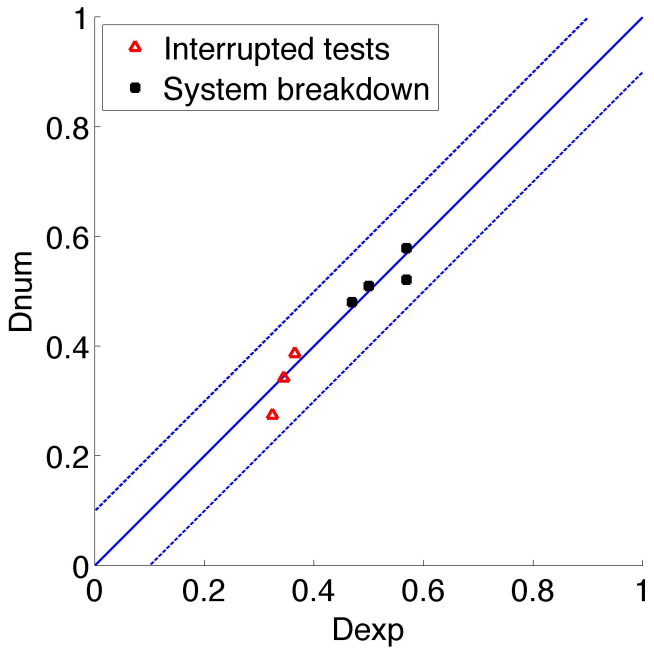

Figure 11: Model versus experiment damage valuefor cyclic oxidation(total damage analysis). Dot lines represent ±10% of error.

stress component associated to the normal direction is used across the whole computation:

- be $\underset{\sim}{\boldsymbol{\sigma}}_s(t)$ the substrate stress history defined in the global axis frame for the considered node,
- the maximum stress level is defined for this node using the equivalent Von Mises stress invariant σ_{eq} : $\underset{\sim}{\boldsymbol{\sigma}}_s^{\max} = \underset{\sim}{\boldsymbol{\sigma}}_s(t_{\max})$ with $t_{\max} = \max_t \sigma_{eq}(t)$,
- the normal direction is the one that minimise the component $\sigma_s^{33}(t_{max})$ for the maximum stress value. This criterion respects the assumption that the local stress state is planar.

Thus a rotation is applied to $\underset{\approx}{\boldsymbol{\varepsilon}}_s$ to estimate substrate strain value in the local tangent plane $\underset{\approx}{\boldsymbol{\varepsilon}}_{sp}$.

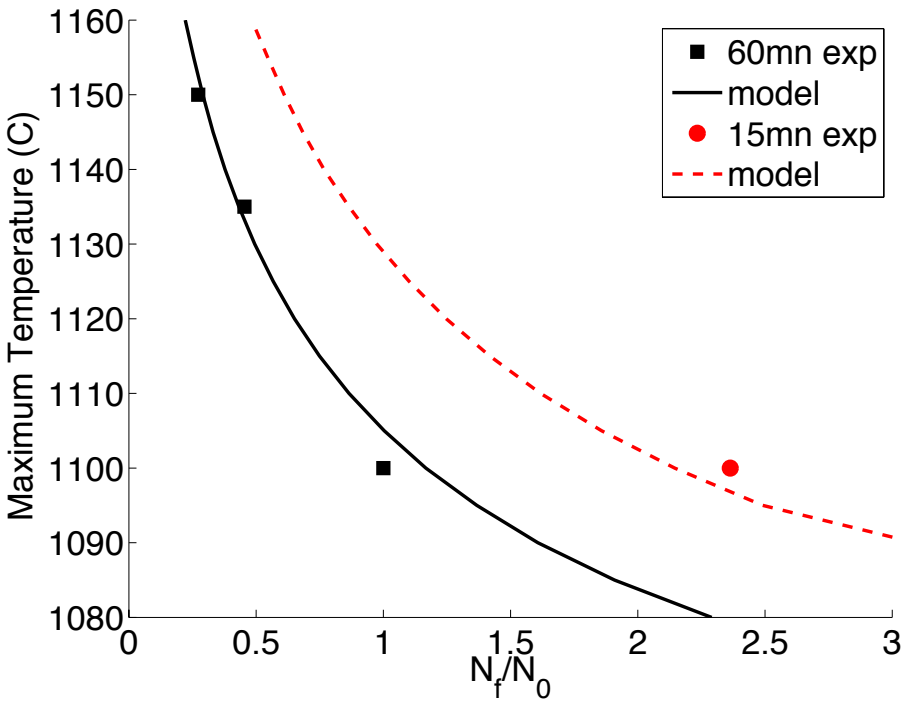

Figure 12: Normalised mean values of cycles to failure as a function of maximum temperature and dwell timefor cyclic oxidation : comparison between model and experiment.

Multi-layer TBC system mechanical state. With the nodal value of $\underset{\sim}{\varepsilon}_{sp}$, bond coat and top coat strain values are computed using the above set of equations 1 to 2. Thus the input parameter ε_{cum} used in equation 11 to estimate the damage related to rumpling, D_r is directly obtained. Whereas, critical strain ε_{crit} used in equation 7 should be estimated with the maximum principal compressive strain in the blade plane.

Damage model and failure analysis. With the above considerations, interfacial damage modelling is undertaken without modification of damage equation, eq. 10 to 12, or new identification of the model parameters. The system failure criterion becomes: the system fails if the maximum absolute value of principal compressive strain exceeds the critical strain ε_{crit}, eq. 7.

The whole post-processor is written in C++ oriented object code, Zset [62, 63].

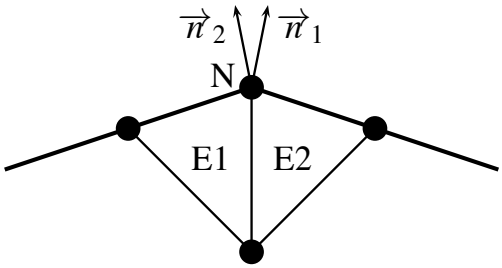

Figure 13: Mesh surface case where normal indetermination should be resolved : two elements with one common edge

4.3. Results for a blade component subjected to TMF loading

The above model is applied as a post-processor on a real blade computation. This case includes TMF loading with high frequency transient for temperature as well as for mechanical loading, courtesy of Snecma-Safran Group. For sake of confidentiality neither the explicit loading path nor the mesh could be included in this paper. Nevertheless, typical loading conditions are sketched Fig. 2, with specific cycling effects in the hottest part of the cycle and with a maximum compressive strain and stress state experienced by the ceramic top coat layer in the low temperature stage.

The results obtained, Fig. 15, are very satisfying as in service damage location is clearly reproduced. Moreover, the model is able to qualitatively describe the spalled area fraction evolution observed for in-service blade under TMF loading for the propagation stage and stabilisation of the spalled area fraction in the second stage, Fig. 15c) [64]. For the time being the model is ratherconservative, and improvement is underway.

5. Discussion

Interrupted tests with mechanical compression are a key-point in TBC life assessment. Indeed, to quantitatively estimate the evolution of interfacial properties, all tests results are discussedthrough an elastic buckling analysis [56]. For TBC systems the direct link made between elastic buckling and final spallation of the ceramic top coat is assumed by most authors. Nevertheless, this methodology uses a damage approach to quantify the global decrease of

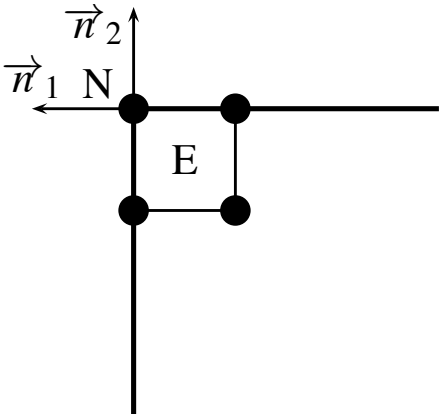

Figure 14: Mesh surface case where normal indetermination should be resolved : single element in edge configuration.

interfacial adherence/toughness between the top coat and the bond coat layers. The damage modes established with our experimental database are close to observations made for real components, validating the chosen experimental procedure.

Indeed, the damage law describes only slow and progressive interfacial damage, whereas elastic buckling analysis is related to the description of final dynamic spallation. Firstly, it enables one to differentiate the time scale related to each phenomenon. Secondly, the related scale in space is very different: damage is initiated from voids, the typical length of which varies from a few microns to large scale buckling of about a few centimetres.

Careful analysis of microscopic features involved in both isothermal and cyclic loading helps to model macroscopic damage evolution D_{ox} and D_r, respectively isothermal and thermal cycling damage terms. It looks as if the top coat/TGO and TGO/bond coat interfaces could be seen as a global damageable inter-phase scale more or less geometrically identical to the TGO layer. The assumption used for the elastic equi-biaxial stress state in the loaded blister is sufficient to describe the macroscopic scale and to account for final breakdown of the system. Lastly the behaviour of the multi-layer system is over-simplified, ignoring the roughness influence on the local stress state which is often modelled in literature using a microstructural FEA or analytical description of a typical wavy pattern [65]. Nevertheless, the above model

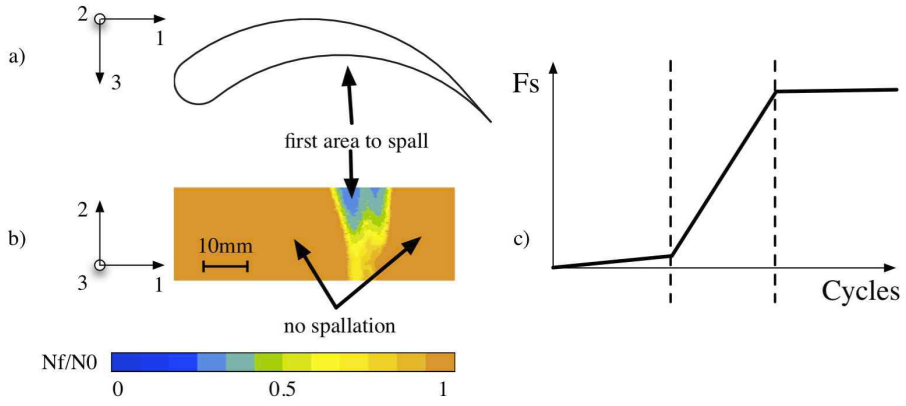

Figure 15: Post-processing made for a 3D blade simulation under TMF loading a) sketch of the blade cross-section b) Detail of a blade surface with iso-values of relative number of cycles at failure Nf. For Nf/N0 =1, no failure is expected to occur. c) Spalled area fraction obtained as a function of the number of cycles.

describes compressed energy available in the system for buckling, whereas the damage approach implicitly accounts for progressive interfacial delamination initiated in the out-of-plane cracking mode.

6. Conclusion

This paper presents an original TBC lifing methodology experimentally based on the analysis of ceramic top coat/metallic bond coat interfacial damage leading to the macroscopic breakdown of the ceramic layer. Temperature is seen as a first order parameter for both spatial scales involved in the TBC system life. At the lower scale the high temperature stage will promote oxide/bond coat interfacial damage due to segregation effect whereas cyclic loading down to the low temperature stage will activate plastic ratchetting leading to a rumpling effect. At the upper scale, the macroscopic spallation is reached in the lowest temperature range or at least on cooling.

Thus, interrupted tests allow one to carefully identify damage mechanism kinetics and life model parameters thanks to the distinction made between, on the one hand, ageing and local interfacial damage and, on the other, macroscopic buckling. The proposed lifetime model for EB-PVD thermal barrier coating complies with industrial purpose and is based on i) the macroscopic buckling condition and ii) a local damage approach related to the oxidation

phenomena and rumpling of the bond coat. The chosen damage approach underlinesthe influence of thermal parameters as well as frequency effects. Hence a good qualitative description of the increase in a spalled area for blade computation is obtained for TMF loading conditions. Moreover this approach is able to qualitatively describe spallation patterns observed in in-service loading on blades.

Diffusion, creep and phase transformation greatly influence BC behaviour, morphology and therefore local stress-strain state. Such effects will be included in a further version of this model. Lastly, all assumptions made for damage mechanisms and the simple mechanical description of the multilayer system are a very promising way to model location of spallation and life assessment for real turbine blades.

Acknowledgments

This work was funded by the Snecma/Safran Group which is gratefully acknowledged. The authors are very grateful to J.-Y. GuÃ©dou (Snecma) for his support.

References

[1] A. G. Evans, D. R. Mumm, J. W. Hutchinson, G. H. Meier, F. S. Pettit, Mechanisms controlling the durability of thermal barrier coatings, Progress in Materials Science 46 (5) (2001) 505 – 553. doi:DOI:10.1016/S0079-6425(00)00020-7.
URL http://www.sciencedirect.com/science/article/B6TX1-4372WDK-2/2/528639fddb36aca05a09a653d333d3b2

[2] S. R. Choi, J. W. Hutchinson, A. G. Evans, Delamination of multilayer thermal barrier coatings, Mechanics of Materials 31 (7) (1999) 431 – 447. doi:DOI:10.1016/S0167-6636(99)00016-2.
URL http://www.sciencedirect.com/science/article/B6TX6-48CPFV5-N/2/fc077f0e1646800e396aafcedad1639a

[3] I. Spitsberg, D. Mumm, A. Evans, On the failure mechanisms of thermal barrier coatings with diffusion aluminide bond coatings, Materials Science and Engineering A 394 (1-2) (2005) 176 – 191. doi:DOI:10.1016/j.msea.2004.11.038.
URL http://www.sciencedirect.com/science/article/B6TXD-4F7H57S-4/2/281c10841b390c75d6f32320f828a3f9

[4] M. Harvey, C. Courcier, V. Maurel, L. Remy, Oxide and tbc spallation in [beta]-nial coated systems under mechanical loading, Surface and Coatings Technology 203 (5-7) (2008) 432 – 436. doi:DOI:10.1016/j.surfcoat.2008.07.037.
URL http://www.sciencedirect.com/science/article/pii/S0257897208006683

[5] L. Remy, Thermal-mechanical fatigue (including thermal shock), in: I. Milne, R. O. Ritchie, , B. Karihaloo (Eds.), Comprehensive Structural Integrity, Pergamon, Oxford, 2003, pp. 113 – 199. doi:DOI:10.1016/B0-08-043749-4/05021-7.

[6] N. Yanar, F. Pettit, G. Meier, Failure characteristics during cyclic oxidation of yttria stabilized zirconia thermal barrier coatings deposited via electron beam physical vapor deposition on platinum aluminide and on nicocraly bond coats with processing modifications for improved performances, Metallurgical and Materials Transactions A 37 (5) (2006)

1563–1580.
URL http://dx.doi.org/10.1007/s11661-006-0100-4

[7] V. Tolpygo, D. Clarke, Temperature and cycle-time dependence of rumpling in platinum-modified diffusion aluminide coatings, Scripta Materialia 57 (7) (2007) 563 – 566. doi:DOI:10.1016/j.scriptamat.2007.06.031.
URL http://www.sciencedirect.com/science/article/B6TY2-4P6MC4C-4/2/c9ba86f742af4e72985fee6f18ee902a

[8] D. S. Balint, J. W. Hutchinson, Undulation instability of a compressed elastic film on a nonlinear creeping substrate, Acta Materialia 51 (13) (2003) 3965 – 3983. doi:DOI:10.1016/S1359-6454(03)00221-0.
URL http://www.sciencedirect.com/science/article/B6TW8-48S2Y7S-3/2/d761c5f3eafab8a77dbbaf62d473ac21

[9] M. Caliez, J. Chaboche, F. Feyel, S. Kruch, Numerical simulation of EBPVD thermal barrier coatings spallation, Acta Mater. 51 (4) (2003) 1133–1141. doi:{10.1016/S1359-6454(02)00518-9}.

[10] E. Busso, L. Wright, H. Evans, L. McCartney, S. Saunders, S. Osgerby, J. Nunn, A physics-based life prediction methodology for thermal barrier coating systems, Acta Materialia 55 (5) (2007) 1491 – 1503. doi:DOI:10.1016/j.actamat.2006.10.023.
URL http://www.sciencedirect.com/science/article/B6TW8-4MV71TK-1/2/f18431edfd5dff84129033654965e5f6

[11] V. Tolpygo, D. Clarke, K. Murphy, Oxidation-induced failure of EB-PVD thermal barrier coatings, Surf. Coat. Technol. 146-147 (2001) 124–131.

[12] C. A. Barrett, C. E. Lowell, NASA TM 81773 (1981) May.

[13] J. L. Smialek, M. A. Gedwill, P. K. Brindley, Cyclic oxidation of aluminide coatings on ti3al+nb, Scripta Metallurgica et Materialia 24 (7) (1990) 1291 – 1296. doi:DOI:10.1016/0956-716X(90)90344-G.
URL http://www.sciencedirect.com/science/article/B6TY3-48F6GPP-JJ/2/e7c6272bb976a8ca4b8ee614904005df

[14] M. P. Bacos, P. Josso, N. Vialas, D. Poquillon, B. Pieraggi, D. Monceau, J. R. Nicholls, N. Simms, A. Encinas-Oropesa,

T. Ericsson, S. Stekovic, Allbatros advanced long life blade turbine coating systems, Applied Thermal Engineering 24 (11-12) (2004) 1745 – 1753, industrial Gas Turbine Technologies. doi:DOI:10.1016/j.applthermaleng.2003.11.018.
URL http://www.sciencedirect.com/science/article/B6V1Y-4BG3J7D-1/2/75929859074578aeb3857cd9efcc10b3

[15] A. G. Evans, G. B. Crumley, R. E. Demaray, On the mechanical behavior of brittle coatings and layers, Oxidation of Metals 20 (5) (1983) 193–216. URL http://dx.doi.org/10.1007/BF00656841

[16] A. G. Evans, M. Y. He, J. W. Hutchinson, Mechanics-based scaling laws for the durability of thermal barrier coatings, Progress in Materials Science 46 (3-4) (2001) 249 – 271. doi:DOI:10.1016/S0079-6425(00)00007-4.
URL http://www.sciencedirect.com/science/article/B6TX1-42JYVPK-6/2/9d71a2833ad9dc3a5e2bc69a4e4c1ee0

[17] S. Choi, D. Zhu, R. Miller, Fracture behavior under mixed-mode loading of ceramic plasma-sprayed thermal barrier coatings at ambient and elevated temperatures, Engineering Fracture Mechanics 72 (13) (2005) 2144 – 2158. doi:DOI:10.1016/j.engfracmech.2005.01.010.
URL http://www.sciencedirect.com/science/article/B6V2R-4FV9MN0-1/2/77fe453b015d686e1636230674fb2ae5

[18] T. Beck, R. Herzog, O. Trunova, M. Offermann, R. W. Steinbrech, L. Singheiser, Damage mechanisms and lifetime behavior of plasma-sprayed thermal barrier coating systems for gas turbines – part ii: Modeling, Surface and Coatings Technology 202 (24) (2008) 5901 – 5908. doi:DOI:10.1016/j.surfcoat.2008.06.132.
URL http://www.sciencedirect.com/science/article/B6TVV-4STB090-H/2/8cc8f5e04d2e270aeb79a734034be229

[19] A. Bickard, L. Rémy, High temperature fatigue behaviour of a thermal barrier coating on a single crystal superalloy, in: High Temperature Surface Engineering, ENSM Paris, Institute of Materials, 2000, pp. 183–198.

[20] B. Baufeld, E. Tzimas, P. Hahner, H. Mullejeans, S. Peteves, P. Moretto,

Phase-angle effects on damage mechanisms of thermal barrier coatings under thermomechanical fatigue, Scripta Mater. 45 (2001) 859–865.

[21] P. K. Wright, Influence of cyclic strain on life of a pvd tbc, Materials Science and Engineering A 245 (2) (1998) 191 – 200. doi:DOI:10.1016/S0921-5093(97)00850-2.
URL http://www.sciencedirect.com/science/article/B6TXD-3SY3VP8-1H/2/969394fa440bf8add6a702b1eed8ab88

[22] E. Tzimas, H. Mullejans, S. D. Peteves, J. Bressers, W. Stamm, Failure of thermal barrier coating systems under cyclic thermomechanical loading, Acta Materialia 48 (18-19) (2000) 4699 – 4707. doi:DOI:10.1016/S1359-6454(00)00260-3.
URL http://www.sciencedirect.com/science/article/B6TW8-41SK82X-1C/2/6a89e89f1014dcf20c4f454f1f3cd049

[23] A. Peichl, T. Beck, O. Vohringer, Behaviour of an eb-pvd thermal barrier coating system under thermal-mechanical fatigue loading, Surface and Coatings Technology 162 (2-3) (2003) 113 – 118. doi:DOI:10.1016/S0257-8972(02)00698-9.
URL http://www.sciencedirect.com/science/article/B6TVV-4771BDH-1/2/13dda186c839eb792abb508b21584228

[24] A. Karlsson, J. Hutchinson, A. Evans, The displacement of the thermally grown oxide in thermal barrier systems upon temperature cycling, Mater. Sci. Engng. A351 (2003) 244–257.

[25] T. S. Hille, T. J. Nijdam, A. S. Suiker, S. Turteltaub, W. G. Sloof, Damage growth triggered by interface irregularities in thermal barrier coatings, Acta Materialia 57 (9) (2009) 2624 – 2630. doi:DOI:10.1016/j.actamat.2009.01.022.
URL http://www.sciencedirect.com/science/article/B6TW8-4VWKPVB-1/2/f28b4f615178a7866747a4cec7ffa145

[26] M. Taylor, H. Evans, C. Ponton, J. Nicholls, A method for evaluating the creep properties of overlay coatings, Surf. Coat. Technol. 124 (2000) 13–18.

[27] A. Volinsky, N. Moody, W. Gerberich, Interfacial toughness measurements for thin films on substrates, Acta Mater. 50 (2002) 441–466.

[28] K. Chan, N. Cheruvu, G. Leverant, Coating life prediction under cyclic oxidation conditions, Journal of Engng for Gas Turbines and Power - Trans. ASME 120 (3) (1998) 609–614, 42nd International Gas Turbine and Aeroengine Congress and Exhibition, Orlando, Florida, JUN 02-05, 1997.

[29] R. Miller, Oxidation-based model for thermal barrier coating life, Journal of the American Ceramic Society 67 (8) (1984) 517 – 521.

[30] T. Cruse, S. Stewart, M. Ortiz, Thermal barrier coating life prediction model development, Trans. ASME (1988) 610–616.

[31] L. Singheiser, R. Steinbrech, W. Quadakkers, R. Herzog, Failure aspects of thermal barrier coatings, Materials at High Temperatures 18 (4) (2001) 249–259.

[32] H. Bernard, L. Rémy, Thermal-mechanical fatigue damage of an aluminide coated nickel-base superalloy, in: H. Exner, V. Schumacher (Eds.), Advanced Materials and Processes, Proceedings of the first European Conference on Advanced Materials and Processes, EUROMAT 89, Paris, Ecole Nationale Superieure des Mines, Evry, France, DGM Informationsgesellschaft, Oberursel, Federal Republic of Germany, 1990, pp. 529–534.

[33] C. Guerre, R. Molins, L. Rémy, Alumina scale growth and degradation modes of a TBC system, Mater. High Temp. 20 (4) (2003) 481–485. doi:{10.3184/096034003782750268}.

[34] A. Bickard, Endommagement sous sollicitations thermiques et mécaniques d'une barriere thermique et d'un aluminiure de nickel déposés sur un superalliage monocristallin, in french, Ph.D. thesis, Ecole des Mines de Paris, France (1998).

[35] C. Guerre, Etude des mécanismes d'endommagement d'un systeme barriere thermique déposé sur un superalliage base nickel, in french, Ph.D. thesis, Ecole des Mines de Paris, France (2002).

[36] I. Rouzou, R. Molins, L. Remy, F. Jomard, Study of the sulfur segregation for a TBC system, in: Steinmetz, P and Wright, IG and Meier, G and Galerie, A and Pieraggi, B and Podor, R (Ed.), HIGH TEMPERATURE CORROSION AND PROTECTION OF MATERIALS 6, PRT 1

AND 2, PROCEEDINGS, Vol. 461-464 of Mater. Sci. Forum, 2004, pp. 101–108, 6th International Symposium on High Temperature Corrosion and Protection of Materials, Les Embiez, FRANCE, MAY 16-21, 2004.

[37] R. Molins, C. Guerre, L. Rémy, Microstructural and chemical TEM characterization of a thermal barrier system, La Revue de Métallurgie-CIT/Science et Génie des Matériaux (2003) 507–512.

[38] A. Koster, E. Fleury, E. Vasseur, L. Rémy, Thermal-mechanical fatigue testing. in: Automation in fatigue and fracture: Testing and analysis (edited by c. amzallag), ASTM STP 1231 (1994) 563–580.

[39] V. Maurel, A. Koster, L. Rémy, An analysis of thermal gradient impact in thermal mechanical fatigue testing, Fatigue Fract. Engng. Mater. Struct. 33 (8) (2010) 473–489.

[40] I. Rouzou, R. L., R. Molins, Internal report Centre des Matériaux - Mines ParisTech (2008).

[41] D. R. Mumm, A. G. Evans, On the role of imperfections in the failure of a thermal barrier coating made by electron beam deposition, Acta Materialia 48 (8) (2000) 1815 – 1827.

[42] J. Wareing, Creep-fatigue behaviour of four casts of type 316 stainless steel, Fatigue and Fracture of Engineering Materials and Structures 4 (1981) 131–145.

[43] V. Tolpygo, D. Clarke, Surface rumpling of a (ni,pt)al bond coat induced by cyclic oxidation, Acta Mater. 48 (2000) 3283–3293.

[44] Y. H. Sohn, J. H. Kim, E. H. Jordan, M. Gell, Thermal cycling of eb-pvd/mcraly thermal barrier coatings: I. microstructural development and spallation mechanisms, Surface and Coatings Technology 146-147 (2001) 70 – 78.

[45] B. A. Pint, On the formation of interfacial and internal voids in α-al2o3 scales, Oxidation of Metals 48 (3) (1997) 303–328.
URL http://dx.doi.org/10.1007/BF01670505

[46] A. Phelippeau, internal report Snecma - Safran Group (2006).

[47] R. Panat, K. Hsia, Experimental investigation of the bond-coat rumpling instability under isothermal and cyclic thermal histories in thermal barrier systems, Proc R Soc Lond Series A - Math Phys Eng Sci 460 (2047) (2004) 1957–1979. doi:{10.1098/rspa.2003.1262}.

[48] S. Darzens, D. Mumm, D. Clarke, A. Evans, Observations and analysis of the influence of phase transformations on the instability of the thermally grown oxide in a thermal barrier system, Metallurgical and Materials Transactions A: Physical Metallurgy and Materials Science 34 A (3) (2003) 511–522.
URL http://www.scopus.com/inward/record.url?eid=2-s2.0-0037353689&partnerID=40

[49] G. Meier, F. Pettit, High-Temperature Corrosion of alumina-forming coatings for superalloys, Surface and Coatings Technology 39 (1-3) (1989) 1–17, 16th International Conference on Metallurgical Coatings (ICMC), San Diego, CA, APR 17-21, 1989.

[50] D. Miracle, Overview no. 104 the physical and mechanical properties of NiAl, Acta Metallurgica et Materialia 41 (3) (1993) 649 – 684. doi:DOI:10.1016/0956-7151(93)90001-9.
URL http://www.sciencedirect.com/science/article/B7599-48CXFM8-19/2/1aadd83850ca2eca2336682904195bd5

[51] M. Caliez, F. Feyel, S. Kruch, J. Chaboche, Oxidation induced stress fields in an EB-PVD thermal barrier coating, Surface and Coatings Technology 157 (2-3) (2002) 103–110.

[52] M. Schütze, Protective oxyde scales and their breakdown, D.R Holmes, Wiley Series on Corrosion and Protection, 1997.

[53] J. Lemaitre, J. L. Chaboche, Mechanics of Solid Materials, Cambridge University Press, 1990.

[54] P. Y. Thery, M. Poulain, M. Dupeux, M. Braccini, Spallation of two thermal barrier coating systems: experimental study of adhesion and energetic approach to lifetime during cyclic oxidation, Journal of Materials Science 44 (7) (2009) 1726–1733. doi:{10.1007/s10853-008-3108-x}.

[55] J. Hutchinson, Z. Suo, Mixed mode cracking in layered materials, Vol. 29 of Advances in Applied Mechanics, Elsevier, 1991, pp. 63 – 191.

doi:DOI:10.1016/S0065-2156(08)70164-9.
URL http://www.sciencedirect.com/science/article/B7RNC-4S867PY-7/2/49133e3f26bd5f190114db2a78ea090d

[56] J. Hutchinson, M. Thouless, E. Liniger, Growth and configurational stability of circular, buckling-driven film delaminations, Acta Metallurgica et Materialia 40 (2) (1992) 295 – 308. doi:DOI:10.1016/0956-7151(92)90304-W.
URL http://www.sciencedirect.com/science/article/B7599-48CXHGY-PT/2/87022e2d285c516d0f143d9fcb220e20

[57] B. Audoly, Mode-dependent toughness and the delamination of compressed thin films, J. Mech. Phys. Solids 48 (11) (2000) 2315–2332.

[58] Y. Rabotnov, Creep rupture, Springer Berlin, 2004, pp. 342–349, 12th International Congress of Applied Mechanics.

[59] H. Lau, C. Leyens, U. Schulz, C. Friedrich, Influence of bondcoat pretreatment and surface topology on the lifetime of EB-PVD TBCs, Surf. Coat. Technol. 165 (3) (2003) 217–223.

[60] C. Wagner, Theorical Analysis of the Diffusion Processes Determining the Oxidation Rate of Alloys, Journal of the Electrochimical Society 99 (10) (1952) 369–380.

[61] M. Wen, E. H. Jordan, M. Gell, Effect of temperature on rumpling and thermally grown oxide stress in an eb-pvd thermal barrier coating, Surface and Coatings Technology 201 (6) (2006) 3289 – 3298. doi:DOI:10.1016/j.surfcoat.2006.07.212.
URL http://www.sciencedirect.com/science/article/B6TVV-4KSSW37-D/2/30ab287de59040fc4b54e6408fb45210

[62] J. Besson, R. Foerch, Large scale object-oriented finite element code design, Comp. Methods Appl. Mech. Engrg. 142 (1997) 165–187.

[63] S. Quilici, Internal report Snecma - Safran Group (2008).

[64] A. G. Evans, D. Clarke, C. Levi, The influence of oxides on the performance of advanced gas turbines, Journal of the European Ceramic Society 28 (2008) 1405–1419.

[65] D. Balint, J. Hutchinson, An analytical model of rumpling in thermal barrier coatings, Journal of the Mechanics and Physics of Solids 53 (4) (2005) 949 – 973. doi:DOI:10.1016/j.jmps.2004.11.002.
URL http://www.sciencedirect.com/science/article/B6TXB-4F6D76V-1/2/0fa1a117b743b6e0f0b919a9c7f0b3a8